

Pressure-softening of zone-edge TA phonons and the fourfold to sixfold phase change

B. A. Weinstein *

Department of Physics, SUNY at Buffalo, 239 Fronczak Hall, Buffalo, New York 14260-1500, USA



(Received 3 May 2021; accepted 15 July 2021; published 4 August 2021)

The observed tendency in tetrahedral solids for the pressure-induced softening of zone-edge TA phonons to correlate with the threshold pressure P_T of the fourfold to sixfold phase change is examined for 25 materials. A strong correlation is found for an effective pressure shift obtained by using a simple tight-binding model to exclude the *frequency-stiffening* non-central-force contribution to the zone-edge TA modes. The correlation is further improved by accounting for the material's shear rigidity. A parameter P_T^{comel} is defined that correlates linearly to P_T with *near-unity slope and high quality factor* up to the transition of BP at ~ 1.6 Mbar. The pressure-softening of the zone-edge TA modes is driven by the negative tension produced in the bonds by compression. This tension originates from increased electron-overlap repulsion, which modifies the metallic and ionic character of the bonding, leading eventually to the phase change. This is the underlying mechanism that links the pressure-softening of the zone-edge TA phonons to the phase transition.

DOI: [10.1103/PhysRevB.104.054105](https://doi.org/10.1103/PhysRevB.104.054105)

I. INTRODUCTION

The pressure-induced phase transitions in tetrahedral crystals can provide insight into the competition among bonding forces to form different high-density structures. In diamond, zinc blende, and wurtzite structure solids, the lowest hydrostatic-pressure transition entails, in general, a change from fourfold to sixfold coordination. (See Ref. [1] and citations therein.) The transformed lattice depends on the material's ionicity—tetragonal β -Sn structure for group IV materials, orthorhombic $Cmcm$ structure for many of the III-V's, and cubic rocksalt structure for the group III nitrides and most of the II-VI's [2]. These transitions are first order in character, exhibiting large discontinuities in volume ($\sim 10\%$ – 20%) and enthalpy brought on by the fourfold to sixfold bonding change. The structural changes proceed by nucleation, and are often reversible. At room temperature the macroscopic growth of transformed domains is frequently sluggish, contributing to pressure hysteresis between the observed forward and reverse transitions [3].

In a large majority of these solids, the frequencies of transverse acoustic phonons belonging to the lowest-frequency TA branch exhibit negative pressure coefficients over wide regions of the Brillouin zone [4–7]. This softening generally occurs for modes extending from the zone edge to deep inside the zone, and often to the $\mathbf{q} \sim 0$ sound waves along directions that correspond to strains of various symmetries [8,9]. The effect of compression on the frequency ν_i of a mode i is often expressed in terms of the mode Grüneisen parameter γ_i defined by

$$\gamma_i \equiv -\left(\frac{\partial \ln \nu}{\partial \ln V}\right)_i = B_o \left(\frac{\partial \ln \nu}{\partial P}\right)_i, \quad (1)$$

where B_o is the bulk modulus.

Early pressure-Raman studies by the present author found an approximate linear correlation between the negative γ_i of the zone-edge TA(X) phonons and the forward onset pressure P_T of the fourfold to sixfold transitions in Si, GaP, ZnS, ZnSe, and ZnTe [4,10]. This correlation was subsequently tested in experiments on Ge, GaAs, InP, and two zinc-blende-like chalcopyrites (chp) CuGaS₂ and AgGaS₂ [11,12]. Arora used the reported pressure data for 12 semiconductors to examine both γ_i and B_o/γ_i for linear relationships between mode-softening and P_T [13]. More recently a correlation test on γ_i was extended to much higher pressures using Raman results on SiC, AlN, GaN, and BeO [14]. For the latter solids, it was found that mode-softening was either weak or absent ($\gamma_i > 0$), and these materials could not be fit into the approximate linear pattern noted for γ_i vs P_T at lower pressures. These subsequent studies concluded that the correlation originally proposed in Ref. [10] had only limited applicability.

Evidence has emerged that the transition mechanism of the fourfold to sixfold change in these materials involves an intermediate metastable state that carries the lattice between its equilibrium end structures. Experiments and *ab initio* calculations indicate that this state forms in < 100 ps via shear-strain distortions, for which the corresponding $\mathbf{q} \sim 0$ TA phonons soften with pressure [e.g., strains dominated by (C_{11} - C_{12})] [15–17]. Orthorhombic or tetragonal metastable states appear to offer the most likely transition paths. Given the evidence for these states, it was found in Ref. [8] that the zone-edge TA softening bears only an indirect relation to the transition. In this view the pressure response of the zone-edge TA phonons merely serves as an approximate gauge of the general softening across the lowest TA branch.

The question remains: To what extent are the *underlying changes in bonding forces* that raise the free energy of the fourfold phase relative to the sixfold phase reflected in the softening of the zone-edge TA modes? This is the issue addressed here. The present study explores in greater detail the approximate correlation between the observed P_T and

*Corresponding author: phyberni@buffalo.edu

the pressure-softening of zone-edge (or zone-edge-like; see below) TA phonons. The available data for 25 tetrahedral materials are surveyed, including also results from different researchers on the same material or its isotope-pure variants. The study differs from prior analyses of this correlation in several ways. (1) Operationally, the analysis focuses on $(\partial \ln \nu / \partial P)_i$ which (rather than γ_i) is usually the primary measured pressure shift. (2) The quantity $(\partial \ln \nu / \partial P)_i$ is modified to account for competing forces, retaining only the part responsible for softening. (3) The shear modulus G is explicitly included in the correlation test. One finds that the results reinforce the rationale for connecting zone-edge TA mode-softening to the phase transitions.

II. APPROACH

For simplicity the generic notation TA(ze) is used to signify the modes that are considered in the present P_T -correlation test. For all the fcc crystals (except 3C-SiC), TA(ze) denotes phonons from the flat section of the lowest TA branch spanning the X to K points. [In 3C-SiC the TA(L) mode is used; its pressure shift is generally similar to that of TA(X , K) in zinc blende compounds.] In hexagonal wurtzite (wz) and tetragonal chalcopyrite (chp) materials, respectively, the E_2 and Γ_5 optical modes at $\mathbf{q} \sim 0$ are zone-folded analogs of the zone-edge TA phonons in fcc structures [18,19]. These zone-folded modes are L -like (in wz) and X -like (in chp), and the pressure-softening of their Raman frequencies is used to include wz and chp crystals in an expanded P_T -correlation test.

Dimensionally, it makes sense to look for a *linear* relationship of P_T with the quantity $(-\partial \ln \nu / \partial P)_{\text{TA(ze)}}^{-1}$, rather than with $\gamma_{\text{TA(ze)}}$ [13]. This approach is pursued here. However, it becomes problematic for materials such as BP, AlN, and BeO in which the zone-edge (or zone-edge-like) TA frequencies have positive pressure shifts [14,20]. This implies an unrealistic discontinuity in the correlation between P_T and $(-\partial \ln \nu / \partial P)_{\text{TA(ze)}}^{-1}$.

To overcome this, the experimental values of $(\partial \ln \nu / \partial P)_{\text{TA(ze)}}$ are adjusted in a physically meaningful way. Consider specifically the important TA(X) and TA(L) modes. Xu *et al.* [21] employ a tight-binding treatment to show that the main contributions to the Grüneisen parameters of these bond-bending modes in group IV solids lead to the expression

$$\gamma = \frac{2}{3} - \frac{4C B_o d_o}{\sqrt{3} m \omega_o^2}, \quad (2)$$

with d_o the bond length, ω_o the phonon angular frequency, m the atomic mass, and $C = 1$ or 2 for TA(L) or TA(X). The first right-hand term acts to stiffen the phonon frequency with pressure, whereas the second term softens the frequency. The stiffening term arises from noncentral angular forces. In the bond-orbital model, the energy associated with a change $\delta\theta$ of the bond angle is $\Delta\varepsilon \sim \langle \eta \rangle (\delta\theta)^2$. Here $\langle \eta \rangle$ is a matrix element between bond orbitals. $\langle \eta \rangle$ varies as $1/d_o^2$, and $\delta\theta \approx u/d_o$ for atomic displacement u . Hence, the noncentral interactions give rise to a force constant $k_\theta \sim d_o^{-4}$, yielding the term $2/3$ in Eq. (2). This term is independent of material parameters.

TABLE I. Values used here for the bulk modulus B_o , the shear modulus G , and the ratio G/B_o . All values derive from measured elastic constants unless *theory* is indicated. The data source is Ref. [25] except where noted.

Material (structure)	B_o (GPa) Reuss	G (GPa) Reuss	G/B_o
Si	97.88	64.97	0.66
3C-SiC	221.7 [26]	185.3 [26]	0.84
Ge	68.87	54.18	0.79
BP	162 [20]	160 ^a [20,27]	0.99
	<i>theory</i>	<i>theory</i>	
AlN (wz)	210.4 [28]	132.7 [28]	0.63
AIP	89.73 [29]	45.07 [29]	0.50
	<i>theory</i>	<i>theory</i>	
AlSb	58.17	30.50	0.52
GaN (wz)	210.8 [28]	118.4 [28]	0.56
GaP	88.19	53.40	0.61
GaAs	75.53	44.73	0.59
GaSb	56.27	32.78	0.58
InN (wz)	146.4 [28]	58.45 [28]	0.40
InP	71.10	32.33	0.46
InAs	57.94	27.63	0.48
BeO (wz)	249.4 [30]	158.5 [30]	0.64
ZnO (wz)	142.5	46.20	0.32
ZnS	74.50	27.79	0.37
ZnSe	65.60	27.02	0.41
ZnTe	50.90	22.04	0.43
CdS (wz)	60.64	16.88	0.28
Cd _{0.6} Mn _{0.4} Te	40.33 [31]	12.11 [31]	0.30
CuCl	39.80	8.662	0.22
CuBr	37.77	7.472	0.20
CuGaS ₂ (chp)	97.90 [32], 74.46 [33]	40.41 [32], 24.04 [33]	0.37 ^b
	<i>theory, theory</i>	<i>theory, theory</i>	
AgGaS ₂ (chp)	66.25 [32]	17.32 [32]	0.26

^aThe Reuss value of G here is obtained from the calculated G_V in Ref. [20] scaled by G_R/G_V found in a similar calculation in Ref. [27].

^bAverage from Refs. [32,33].

The second term is due to compression of the bonds; it derives from central forces. Pressure introduces a *negative* (compressive) increment of tension T_P in the bonds. For the bond-bending motions in the TA(X or L) modes, this creates a *counter-restoring* force with spring constant $k_{\text{cent}} = 2CT_P/d_o$. Xu *et al.* obtain the second term in Eq. (2) by equating the elastic compression energy with the work against T_P to uniformly contract the bonds. This is the physical origin of the pressure-induced softening of the zone-edge TA(X or L) modes.

One expects that only the softening component of the zone-edge TA-phonon pressure shift should closely reflect the changes in bonding forces that destabilize the tetrahedral lattice. Consequently, in the present study the test for a correlation between P_T and the softening of zone-edge TA modes is conducted using the modified pressure shift,

$$\left(\frac{\partial \ln \nu}{\partial P} \right)_{\text{TA(ze)}}^* = \left(\frac{\partial \ln \nu}{\partial P} \right)_{\text{TA(ze)}} - \frac{2}{3B_o}, \quad (3)$$

TABLE II. Values used for the transition pressures P_T , frequencies $\nu_{TA(ze)}$, rates of shift $(\partial \ln \nu / \partial P)_{TA(ze)}$, and correlation-test pressure P_T^{correl} . Columns 2–4 are from experiment except as noted. Uncertainty estimates are in parentheses.

Material (structure)	P_T (GPa)	$\nu_{TA(ze)}$ (cm^{-1})	$(\partial \ln \nu / \partial P)_{TA(ze)}$ ($10^{-3}/\text{GPa}$)	P_T^{correl} (GPa)
Si	11.70	151.0 [4,5]	$-13.9(2.7)^a$ [4,5], $-18.0(0.6)^b$ [4,5]	14.7(1.9)
3C-SiC	100.0 [34]	266.0 ^c [11,35]	$-1.89(0.35)^c$ [11,35]	85.3(6.1)
Ge	10.60	81.6 ^d [11], 81.5 ^e [11] 83.0 [6]	$-16.0(0.4)^d$ [11], $-20.6(0.7)^e$ [11] $-17.6(2.0)$ [6]	14.2(1.2)
BP	160.0 [36] <i>theory</i>	310.5 [20]	+1.10 [20]	164
AlN (wz)	22.90 [37]	247.2 ^f [14,38,39]	+0.32(0.12) ^f [14,38,39]	111(5.6)
AIP	14.20	137.5 [29] <i>theory</i>	-27.6 [29] <i>theory</i>	7.16
AlSb	8.10	69.5 [40]	$-27.1(2.2)$ [40]	6.79(0.39)
GaN (wz)	52.20 [41] 48.00 [18]	144.0 ^g [39,18]	$-2.08(0.62)^g$ [39] -1.74^g [18]	55.5(6.6)
GaP	26.00	104.7 [4,5]	$-8.06(0.36)$ [4,5]	19.4(0.4)
GaAs	17.30	80.2 [22] 81.4 [43]	$-15.6(1.2)$ [22], $-21.5(0.7)$ [42] -25.5 [43]	10.2(1.8)
GaSb	7.65	56.5 [7]	$-46.9(2.1)$ [7]	4.96(0.18)
InN (wz)	12.10 [41] 13.50 [45]	88.0 ^g [44]	-4.55^g [44]	21.9
InP	9.80	67.5 [42]	$-28.7(1.4)$ [42]	5.97(0.22)
InAs	7.60	53.0 [46]	-37.6 [47] <i>theory</i>	4.86
BeO (wz)	137.0 [48]	338.0 ^g [49]	+0.19(0.28) ^g [49]	128(14)
ZnO (wz)	9.10	99.0 ^g [50,51]	-9.41^g [50], -11.5^g [51]	10.7(1.1)
ZnS	14.70	90.0 [4,10]	$-19.4(1.9)$ [4,10]	6.58(0.44)
⁶⁸ Zn ³² S	14.70	88.6 [52,53]	$-16.1(1.6)$ [52]	7.44(0.47)
ZnSe	13.00	69.5 [4,10]	$-21.6(0.7)$ [4,10]	6.48(0.14)
⁶⁸ Zn ⁷⁶ Se	13.00	69.5 [54]	$-23.2(0.8)$ [54]	6.17(0.14)
ZnTe	9.50	55.0 [4,10,55]	$-30.5(3.9)$ [4,10], $-30.2(1.3)$ [55]	4.98(0.30)
⁶⁴ Zn Te	9.50	55.1 [54]	$-29.4(2.2)$ [54]	5.10(0.25)
CdS (wz)	2.34	42.0 ^g [51]	-44.8^g [51]	2.49
Cd _{0.6} Mn _{0.4} Te	3.20 [56,57]	42.0 [56]	$-60.0(5.5)$ [56,57]	1.96(0.14)
CuCl	5.10 [58]	34.5 [59]	-36.7 [59,60]	2.04
CuBr	4.80 [58]	36.5 [59]	-10.3 [59,60]	3.54
CuGaS ₂ (chp)	16.50 [12]	75.0 ^h [12], 74.0 ^h [61]	$-8.53(0.43)^h$ [12], -9.46^h [61]	11.1(0.33)
AgGaS ₂ (chp)	4.20 [12]	36.0 ^h [12]	$-72.2(3.6)^h$ [12]	1.59(0.07)

^aFrom best fit of Si data up to 12.1 GPa.

^bFrom best fit of Si data up to 9.0 GPa.

^cFor TA(L) mode.

^dFor $\nu_{TA(X)}$ vs pressure.

^eFor $\nu_{TA(X)}$ vs volume.

^fAverage of the cited results for lowest $\mathbf{q} \sim 0 E_2$ mode.

^gFor lowest $\mathbf{q} \sim 0 E_2$ mode.

^hFor lowest $\mathbf{q} \sim 0 \Gamma_5$ mode.

where the first right-hand term is the experimentally observed shift. This modified shift is negative for the 25 materials studied here, including BP, AlN, and BeO.

One should also take into account the shear rigidity of the material because the observed P_T are elevated by energy barriers associated with shear strain. Two considerations motivate this, the need for shear strain to drive the transitions, and the tendency for rigid materials to resist macroscopic phase growth. Examples are the enthalpy to create an orthorhombic intermediate state in the zinc blende to rocksalt change [16,17], and the mechanical barriers due to grain-boundary-like dislocations at the surface of local transformed domains

during nucleation [3,22]. The ratio of shear to bulk moduli G/B_o is a measure of a material's shear rigidity vs its cohesive strength [23]. It is included in our P_T -correlation test as a factor that increases the test parameter for higher ratio values. B_o and G are obtained using the standard Reuss formulas for the ambient structures [24].

In view of the above considerations, our correlation analysis will compare the measured values of P_T to the test parameter,

$$P_T^{\text{correl}} = -\frac{G}{2B_o} \left\{ \left(\frac{\partial \ln \nu}{\partial P} \right)_{TA(ze)}^* \right\}^{-1}. \quad (4)$$

The factor 2 in the denominator relates Eq. (4) to the pressure variation of a mode's force constant.

III. RESULTS

Tables I and II list the values of the quantities used to compute P_T^{correl} . They are obtained from a survey of the literature for the 25 materials treated in this study. All values are from experiment except in cases where successful measurements are unavailable, which is indicated by including the word *theory* under a cited value. If a substance has the wurtzite (wz) or chalcopyrite (chp) structure at 1 atm, this is noted in parentheses after the material designation. In Table I the bulk and shear moduli are computed from elastic constant data by means of the Reuss approximation expressions [24]; for AlP and CuGaS₂ only theoretical elastic constants were available, and for BP calculated moduli in excellent agreement with recent hardness experiments were used [20]. The Reuss approximation gives a lower limit average for B_o and G in polycrystalline material assuming uniform stress. For uniform strain the Voigt approximation supplies an upper limit. The numerical difference between these limits is generally small. The uniform stress formulation seems most appropriate here, since the transitions proceed by growth of domains that experience large volume reductions and local surface strains.

In Table II the second column lists the observed forward transition pressures P_T . Many of these values are taken from the 2003 review by Mujica *et al.* [1], and are pressures measured in various x-ray experiments, referenced therein. For materials not treated in that review, the P_T values come from other measured data sources, and for BP (P_T not yet measured) from *ab initio* theory, as cited in the table for these substances. The Table II caption and footnotes specify the identities of the TA(ze) modes for the different materials. The 1 atm frequencies $\nu_{\text{TA(ze)}}$ are drawn from Raman or neutron scattering data. In column 4 the fractional pressure shifts $(\partial \ln \nu / \partial P)_{\text{TA(ze)}}$ are mainly from pressure-Raman experiments (except for GaSb and one Ge datum from neutron scattering). Theoretical values are used for $\nu_{\text{TA(ze)}}$ in AlP and for $(\partial \ln \nu / \partial P)_{\text{TA(ze)}}$ in AlP and InAs, again absent measured results in these cases. The uncertainties in the pressure shifts, if stated by the authors, appear in parentheses. The last column lists the values of P_T^{correl} computed via Eqs. (3) and (4). For materials with multiple values of $(\partial \ln \nu / \partial P)_{\text{TA(ze)}}$ in column 4, P_T^{correl} is the resulting average. The listed uncertainties in P_T^{correl} derive from the pressure-shift uncertainties.

The graph in Fig. 1 shows the result of plotting P_T against P_T^{correl} for the 25 materials in this study. The solid line is a linear least square fit to the data, excluding *only* the AlN point. The spread in the data points (many of which overlap) is influenced by uncertainties in both P_T^{correl} and P_T . Estimates of the former appear in Table II for many of the materials; estimates of the latter are difficult because observations of P_T are measurement and sample dependent. Error bars for the uncertainty in P_T^{correl} are included in Fig. 1 where data points would not be obscured. The size of the typical uncertainty in P_T^{correl} is comparable to the deviation of the points from the fitted line, supporting the ability of the data to define correlated behavior. AlN is clearly an exception that does

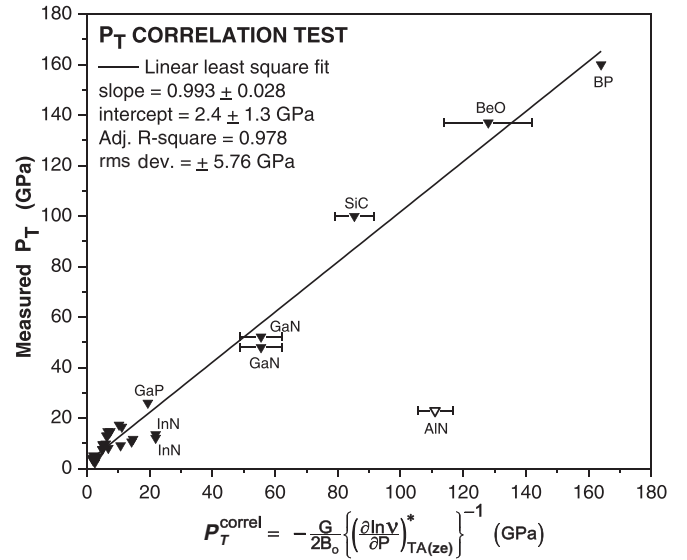


FIG. 1. Plot of the measured pressure P_T for the fourfold to sixfold transition in the 25 considered materials vs P_T^{correl} computed using Eqs. (3) and (4). See Table II for numerical values. Solid line is a linear fit to the data points excluding AlN; best fit parameters are shown at upper left.

not conform to the pattern of the other materials. One might consider whether InN also falls outside this pattern. However, given the uncertainties in P_T^{correl} , and the proximity of GaN to the fitted line, it is appropriate to include InN with the main group. The linear fit in Fig. 1 has a slope close to unity, an intercept near the origin (at $P_T \sim 2.4$ GPa), an Adj. R -square factor of 0.978, and an rms deviation of ± 5.76 GPa. The Fig. 1 results show that P_T^{correl} exhibits a clear linear correlation with the observed transition pressures P_T . Although this correlation is approximate, it nevertheless reveals a strong trend that extends into the megabar regime.

In order to separate and better identify the data points for different materials, Fig. 2 is presented for the reader's convenience. This figure displays a plot of the same data values as in Fig. 1, but on a log-log scale. Likewise, the solid curve in Fig. 2 is the fitted line of the previous figure transferred to the log-log scale. The correlation of the data with the fitted line (excluding AlN) is again apparent.

IV. DISCUSSION

Analysis of the correlated behavior between P_T and P_T^{correl} leads to several insights. The assertion of Lambrecht and his co-workers [8] that the softening of zone-edge TA phonons bears only an indirect relation to the transition is a reasonable starting point. There is no necessary correspondence between the transformed structures and the symmetry of the zone-edge TA modes that undergo the strongest pressure-softening. The strain distortions required to transform the lattices between their equilibrium structures cannot be supplied directly by the zone-edge TA modes. The orthorhombic intermediate states [15–17] considered for the pathways between the zinc blende or the wurtzite and the rocksalt structures require shear strains that involve C_{44} and $(C_{11}-C_{12})$ [9]. Alternatively, it is

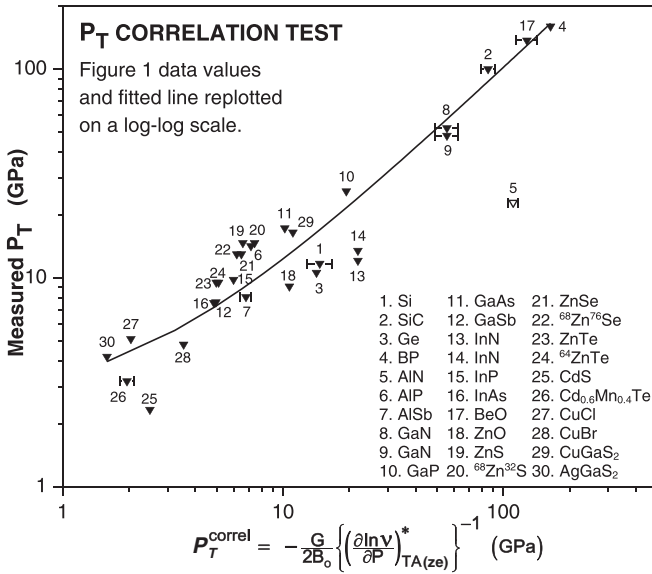


FIG. 2. Plot for clarity on a log-log scale of the same P_T vs P_T^{correl} data points and linear fit as given in Fig. 1. Numbers label the data points according to the material key at lower right.

conceivable that some type of anharmonic interaction might involve the zone-edge TA modes more directly. However, in any case, the correlation in Fig. 1 demonstrates that the softening of the zone-edge (or zone-edge analog) TA(X , K , L) phonons, and the softening of the $q \sim 0$ shear modes that drive the structural changes, originate in the same pressure-induced variation of bonding forces.

Which forces are responsible? The tight-binding model leading to Eq. (2) shows that the balance between central and noncentral nearest-neighbor restoring forces is crucial for the bond-bending zone-edge TA modes. Applied pressure strengthens the noncentral angular restoring forces. In contrast, under pressure the central force contribution causes softening of these bond-bending frequencies due to the compressive (negative) tension induced in the bonds. That is, the softening occurs because the interatomic distance is decreased, and with that change comes increased electron-electron overlap repulsion. This tends to redistribute the valence electron density, modifying the metallic and ionic character of the bonding to different degrees depending on the material's ionicity. The resulting variation in interatomic forces eventually lowers the binding energy of the fourfold phase below that of the sixfold phase, which benefits from its two additional bonds. This qualitative physical picture, based on conventional bonding ideas in tetrahedral solids, is sufficient to justify a link between the phase transition pressure and the quantity $\{(\partial \ln \nu / \partial P)_{\text{TA}(ze)}^*\}^{-1}$.

As anticipated, the factor G/B_0 improves the linear correlation with P_T . Without this factor there is still an approximate linear correlation between P_T and $\{(\partial \ln \nu / \partial P)_{\text{TA}(ze)}^*\}^{-1}$, but it is not as strong. Compared to the fit in Fig. 1, the rms deviation (± 13.6 GPa) is more than two times larger, and the Adj. R -square factor (0.880) is 10% smaller (again AlN is excluded from the fit). Additionally, in Fig. 1, the factor G/B_0 increases the linear slope of the correlation from

~ 0.76 to *near unity*. At present the reason for this fortuitous and intriguing result, implying that $P_T^{\text{correl}} \approx P_T$, is not apparent.

Carbon (diamond) is not included in the present study. Its high-pressure transition has not yet been observed. Detailed first principles calculations show that diamond is stable until ~ 1075 GPa, and then should transform to another fourfold structure (BC8) [62]. This pressure is an order of magnitude above the transition range of the other tetrahedral materials treated here. Nevertheless it is instructive to estimate a value of P_T^{correl} for diamond. The mode Grüneisen parameters of diamond for acoustic and optic modes across the Brillouin zone have been calculated using *ab initio* density-functional theory [63]. For the TA(X) mode the obtained result is $\gamma_{\text{TA}(X)} = +0.28$. Using this value one may estimate P_T^{correl} by means of Eqs. (3) and (4) taking $B_0 = 442.3$ GPa and $G = 531.9$ GPa (Reuss value) from the diamond elastic constants [25]. One obtains $P_T^{\text{correl}} = 684$ GPa for diamond, about 2/3 of the theoretical P_T for transition to the BC8 phase.

The differences between the high-pressure phase and stability of diamond compared to Si and Ge have been attributed to the tightly bound $2p$ orbitals of C, which strongly favor sp^3 bonding in that material [64,65]. Similar considerations apply to the $2p$ orbitals of N in AlN, but there the $3p$ Al orbitals also influence the sp^3 bonding. Diamond and AlN are both materials that fall outside the linear correlation pattern in Figs. 1 and 2. The origin of these deviations requires further study.

V. CONCLUSION

The correlation between the threshold pressure P_T for the fourfold to sixfold transition in tetrahedral crystals and the pressure-softening of their zone-edge TA phonons has been explored for 25 materials. This correlation was proposed based on early pressure-Raman studies [4,10], and the evidence for it has been considered repeatedly with inconclusive findings as to the pressure range, usefulness, and meaning of the observed behavior [8,14]. The present work demonstrates that a strong trend for linear correlation indeed exists between P_T and the softening of zone-edge TA modes, when this softening is expressed in terms of the inverse of an effective fractional pressure shift. The strength and pressure extent of this trend depend on (i) including in the effective pressure shift *only the central-force term that actually causes softening*, and (ii) accounting for the material's shear rigidity. The parameter P_T^{correl} , defined by Eqs. (3) and (4), is constructed to meet these criteria by applying the tight-binding model of Xu *et al.* [21] to remove the noncentral restoring-force term from the measured pressure shifts, and by including the factor G/B_0 . It is found that P_T^{correl} and P_T correlate linearly with near-unity slope and with a high quality factor up to the transitions of BeO and BP in the 1.5 Mbar range. Among the 25 materials surveyed only AlN falls outside of the correlation, as also does a separate estimate for diamond.

In tetrahedral solids the pressure-softening of zone-edge TA modes originates from the negative tension in the bonds induced by compression. This tension arises from increased overlap repulsion, which modifies the charge density

distribution, causing changes in interatomic forces and bonding character that drive the phase transition. These underlying bonding-force changes justify the correlation between the softening of the zone-edge TA modes (as represented by P_T^{correl}) and the threshold P_T of the fourfold to sixfold transition.

ACKNOWLEDGMENTS

The author is indebted to the late Manuel Cardona for drawing his attention in a prior correspondence to the results of Ref. [21] on the origin of the negative Grüneisen parameters of zone-edge TA modes in tetrahedral materials.

- [1] A. Mujica, A. Rubio, A. Munoz, and R. J. Needs, High-pressure phases of group-IV, III-V, and II-VI compounds, *Rev. Mod. Phys.* **75**, 863 (2003).
- [2] V. Ozolins and A. Zunger, Theory of Systematic Absence of NaCl-type (β -Sn-type) High Pressure Phases in Covalent (Ionic) Semiconductors, *Phys. Rev. Lett.* **82**, 767 (1999).
- [3] J. M. Besson, J. P. Itie, A. Polian, G. Weill, J. L. Mansot, and J. Gonzalez, High-pressure phase transition and phase diagram of gallium arsenide, *Phys. Rev. B* **44**, 4214 (1991).
- [4] B. A. Weinstein and R. Zallen, Pressure-Raman effects in covalent and molecular solids, in *Light Scattering in Solids IV*, edited by M. Cardona and G. Guntherodt, Topics in Applied Physics (Springer, Berlin, 1984), Vol. 54, pp. 463–527; see, especially, Table 8.1 and pp. 492–497 in this review.
- [5] B. A. Weinstein and G. J. Piermarini, Raman scattering and phonon dispersion in Si and GaP at very high pressure, *Phys. Rev. B* **12**, 1172 (1975).
- [6] S. Klotz, J. M. Besson, M. Braden, K. Karch, P. Pavone, D. Strauch, and W. G. Marshall, Pressure Induced Frequency Shifts of Transverse Acoustic Phonons in Germanium to 9.7 GPa, *Phys. Rev. Lett.* **79**, 1313 (1997).
- [7] S. Klotz, M. Braden, J. Kulda, P. Pavone, and B. Steininger, Transverse acoustic phonons of GaSb up to 7 GPa by inelastic neutron scattering, *Phys. Status Solidi B* **223**, 441 (2001).
- [8] M. Prikhodko, M. S. Miao, and W. R. L. Lambrecht, Pressure dependence of sound velocities in 3C-SiC and their relation to the high-pressure phase transition, *Phys. Rev. B* **66**, 125201 (2002).
- [9] K. Sarasamak, S. Limpijumnong, and W. R. L. Lambrecht, Pressure-dependent elastic constants and sound velocities of wurtzite SiC, GaN, InN, ZnO, and CdSe, and their relation to the high-pressure phase transition: A first-principles study, *Phys. Rev. B* **82**, 035201 (2010).
- [10] B. A. Weinstein, Phonon dispersion of zinc chalcogenides under extreme pressure and the metallic transformation, *Solid State Commun.* **24**, 595 (1977); in *High-Pressure Science and Technology*, edited by K. D. Timmerhaus and M. S. Barber (Plenum, New York, 1979), Vol. 1, pp. 141–151.
- [11] D. Olego and M. Cardona, Pressure dependence of Raman phonons of Ge and 3C-SiC, *Phys. Rev. B* **25**, 1151 (1982).
- [12] C. Carlone, D. Olego, A. Jayaraman, and M. Cardona, Pressure dependence of the Raman modes and pressure-induced phase changes in CuGaS₂ and AgGaS₂, *Phys. Rev. B* **22**, 3877 (1980).
- [13] A. K. Arora, Grüneisen parameter of soft phonons and high pressure phase transitions in semiconductors, *J. Phys. Chem. Solids* **51**, 373 (1990).
- [14] E. V. Yakovenko, M. Gauthier, and A. Polian, High-pressure behavior of the bond-bending mode of AlN, *Zh. Eksp. Teor. Fiz.* **125**, 1122 (2004) [*J. Exp. Theor. Phys.* **98**, 981 (2004)]; E. V. Yakovenko, M. Gauthier, and A. Polian, [arXiv:cond-mat/0301045v1](https://arxiv.org/abs/cond-mat/0301045v1).
- [15] M. D. Knudson, Y. M. Gupta, and A. B. Kunz, Transformation mechanism for the pressure-induced phase transition in shocked CdS, *Phys. Rev. B* **59**, 11704 (1999).
- [16] M. Catti, First-principles study of the orthorhombic mechanism for the B3/B1 high-pressure phase transition of ZnS, *Phys. Rev. B* **65**, 224115 (2002).
- [17] M. S. Miao and W. R. L. Lambrecht, Universal Transition State for High-Pressure Zinc Blende to Rocksalt Phase Transitions, *Phys. Rev. Lett.* **94**, 225501 (2005).
- [18] P. Perlin, C. Jauberthie-Carillon, J. P. Itie, A. San Miguel, I. Grzegory, and A. Polian, Raman scattering and x-ray absorption spectroscopy in gallium nitride under high pressure, *Phys. Rev. B* **45**, 83 (1992).
- [19] J. P. van der Ziel, A. E. Meixner, H. M. Kasper, and J. A. Ditzenberger, Lattice vibrations of AgGaS₂, AgGaSe₂, and CuGaS₂, *Phys. Rev. B* **9**, 4286 (1974).
- [20] R. Gui, Z. Xue, X. Zhou, C. Gu, X. Ren, H. Cheng, D. Ma, J. Qin, Y. Liang, X. Yan, J. Zhang, X. Zhang, X. Yu, L. Wang, Y. Zhao, and S. Wang, Strain stiffening, high load-invariant hardness, and electronic anomalies of boron phosphide under pressure, *Phys. Rev. B* **101**, 035302 (2020).
- [21] C. H. Xu, C. Z. Wang, C. T. Chan, and K. M. Ho, Theory of the thermal expansion of Si and diamond, *Phys. Rev. B* **43**, 5024 (1991).
- [22] U. D. Venkateswaran, L. J. Cui, B. A. Weinstein, and F. A. Chambers, Forward and reverse high-pressure transitions in bulklike AlAs and GaAs epilayers, *Phys. Rev. B* **45**, 9237 (1992).
- [23] S. Kamran, K. Chen, and L. Chen, Semiempirical formulae for elastic moduli and brittleness of diamondlike and zinc-blende covalent crystals, *Phys. Rev. B* **77**, 094109 (2008).
- [24] Z. Wu, E. Zhao, H. Xiang, X. Hao, X. Liu, and J. Meng, Crystal structures and elastic properties of superhard IrN₂ and IrN₃ from first principles, *Phys. Rev. B* **76**, 054115 (2007); A. Reuss, *Z. Angew. Math. Mech.* **9**, 49 (1929).
- [25] *Semiconductors—Basic Data*, 2nd rev. ed., edited by O. Madelung (Springer-Verlag, Berlin, 1996).
- [26] K. K. Zhuravlev, A. F. Goncharov, S. N. Tkachev, P. Dera, and V. B. Prakapenka, Vibrational, elastic, and structural properties of cubic silicon carbide under pressure up to 75 GPa: Implication for a primary pressure scale, *J. Appl. Phys.* **113**, 113503 (2013).
- [27] X. Zhang, J. Qin, H. Liu, S. Zhang, M. Ma, W. Luo, R. Liu, and R. Ahuja, Pressure-induced zigzag phosphorus chain and superconductivity in boron monophosphide, *Sci. Rep.* **5**, 8761 (2015).
- [28] K. Kim, W. R. L. Lambrecht, and B. Segall, Elastic constants and related properties of tetrahedrally bonded BN, AlN, GaN, and InN, *Phys. Rev. B* **53**, 16310 (1996).

- [29] S. Aouadi, P. Rodriguez-Hernandez, K. Kassali, and A. Munoz, Lattice dynamics properties of zinc-blende and nickel arsenide phases of AlP, *Phys. Lett. A* **372**, 5340 (2008).
- [30] G. G. Bentle, Elastic constants of single-crystal BeO at room temperature, *J. Am. Ceram. Soc.* **49**, 125 (1966).
- [31] P. Maheswaranathan, R. J. Sladek, and U. Debska, Elastic constants and their pressure dependences in $\text{Cd}_{1-x}\text{Mn}_x\text{Te}$ with $0 \leq x \leq 0.52$ and in $\text{Cd}_{0.52}\text{Zn}_{0.48}\text{Te}$, *Phys. Rev. B* **31**, 5212 (1985); data from this reference for $\text{Cd}_{0.55}\text{Mn}_{0.45}\text{Te}$ are used in the present study.
- [32] A. H. Romero, M. Cardona, R. K. Kremer, R. Lauck, G. Siegle, C. Hoch, A. Muñoz, and A. Schindler, Electronic and phononic properties of the chalcopyrite CuGaS_2 , *Phys. Rev. B* **83**, 195208 (2011).
- [33] A. K. Kushwaha, R. Khenata, A. Bouhemadou, S Bin-Omran, and K. Haddadi, Lattice dynamical properties and elastic constants of the ternary chalcopyrite compounds CuAlS_2 , CuGaS_2 , CuInS_2 , and AgGaS_2 , *J. Electron. Mater.* **46**, 4109 (2017).
- [34] M. Yoshida, A. Onodera, M. Ueno, K. Takemura, and O. Shimomura, Pressure-induced phase transition in SiC, *Phys. Rev. B* **48**, 10587 (1993).
- [35] A. Debernardi, C. Ulrich, K. Syassen, and M. Cardona, Raman linewidths of optical phonons in 3C-SiC under pressure: First-principles calculations and experimental results, *Phys. Rev. B* **59**, 6774 (1999).
- [36] R. M. Wentzcovitch, M. L. Cohen, and P. K. Lam, Theoretical study of BN, BP, and BAs at high pressures, *Phys. Rev. B* **36**, 6058 (1987).
- [37] M. Ueno, A. Onodera, O. Shimomura, and K. Takemura, X-ray observation of the structural phase transition of aluminum nitride under high pressure, *Phys. Rev. B* **45**, 10123 (1992).
- [38] F. J. Manjon, D. Errandonea, A. H. Romero, N. Garro, J. Serrano, and M. Kuball, Lattice dynamics of wurtzite and rock-salt AlN under high pressure: Effect of compression on the crystal anisotropy of wurtzite-type semiconductors, *Phys. Rev. B* **77**, 205204 (2008).
- [39] A. R. Goni, H. Siegle, K. Syassen, C. Thomsen, and J.-M. Wagner, Effect of pressure on optical phonon modes and transverse effective charges in GaN and AlN, *Phys. Rev. B* **64**, 035205 (2001).
- [40] Y. S. Raptis and K. Syassen, Pressure dependence of zone-boundary phonons in AlSb, *Int. J. High Pressure Res.* **9**, 31 (1992).
- [41] M. Ueno, M. Yoshida, A. Onodera, O. Shimomura, and K. Takemura, Stability of the wurtzite-type structure under high pressure: GaN and InN, *Phys. Rev. B* **49**, 14 (1994).
- [42] R. Trommer, H. Muller, M. Cardona, and P. Vogl, Dependence of the phonon spectrum of InP on hydrostatic pressure, *Phys. Rev. B* **21**, 4869 (1980).
- [43] P. Y. Yu and B. Welber, High pressure photoluminescence and resonant Raman study of GaAs, *Solid State Commun.* **25**, 209 (1978).
- [44] J. Ibanez, F. J. Manjon, A. Segura, R. Oliva, R. Cusco, R. Vilaplana, T. Yamaguchi, Y. Nanishi, and L. Artus, High-pressure Raman scattering in wurtzite indium nitride, *Appl. Phys. Lett.* **99**, 011908 (2011).
- [45] C. Pinquier, F. Demangeot, J. Frandon, J.-C. Chervin, A. Polian, B. Couzinet, P. Munsch, O. Briot, S. Ruffenach, B. Gil, and B. Maleyre, Raman scattering study of wurtzite and rocksalt InN under high pressure, *Phys. Rev. B* **73**, 115211 (2006).
- [46] R. Carles, N. Saint-Cricq, J. B. Renucci, M. A. Renucci, and A. Zwick, Second-order Raman scattering in InAs, *Phys. Rev. B* **22**, 4804 (1980).
- [47] D. N. Talwar and M. Vandevyver, Pressure-dependent phonon properties of III-V compound semiconductors, *Phys. Rev. B* **41**, 12129 (1990).
- [48] Y. Mori, T. Ikai, and K. Takarabe, The phase transition of BeO under high pressure, Photon Factory Activity Report, 2002 No. 20 Part B, High Pressure Science, 13A, 18C/2001G042, 2003.
- [49] A. P. Jephcoat, R. J. Hemley, H. K. Mao, R. E. Cohen, and M. J. Mehl, Raman spectroscopy and theoretical modeling of BeO at high pressure, *Phys. Rev. B* **37**, 4727 (1988); in the present study the Table II value of $[\partial \ln \nu / \partial P]_{E2}$ is obtained as γ_{E2}/B_o from this reference which uses $B_o = 212$ GPa from R. M. Hazen and L. W. Finger, *J. Appl. Phys.* **59**, 3728 (1986).
- [50] F. Decremps, J. Pellicer-Porres, A. M. Saitta, J.-C. Chervin, and A. Polian, High-pressure Raman spectroscopy study of wurtzite ZnO, *Phys. Rev. B* **65**, 092101 (2002).
- [51] S. S. Mitra, O. Brafman, W. B. Daniels, and R. K. Crawford, Pressure-induced phonon frequency shifts measured by Raman scattering, *Phys. Rev.* **186**, 942 (1969).
- [52] R. E. Tallman, Ph.D. dissertation, University at Buffalo, The State University of New York, May, 2009 (unpublished).
- [53] J. Serrano, A. Cantarero, M. Cardona, N. Garro, R. Lauck, R. E. Tallman, T. M. Ritter, and B. A. Weinstein, Raman scattering in β -ZnS, *Phys. Rev. B* **69**, 014301 (2004).
- [54] G. P. Lindberg and B. A. Weinstein, Precipitation of anion inclusions and plasticity under hydrostatic pressure in II-VI crystals, *Phys. Rev. B* **94**, 134102 (2016); G. P. Lindberg, Ph.D. dissertation, University at Buffalo, The State University of New York, March, 2016 (unpublished).
- [55] J. Camacho, I. Loa, A. Cantarero, and K. Syassen, Vibrational properties of ZnTe at high pressures, *J. Phys.: Condens. Matter* **14**, 739 (2002).
- [56] A. K. Arora, D. U. Bartholomew, D. L. Peterson, and A. K. Ramdas, Raman-scattering study of the high-pressure phase transition in $\text{Cd}_{1-x}\text{Mn}_x\text{Te}$, *Phys. Rev. B* **35**, 7966 (1987).
- [57] K. Strossner, S. Ves, W. Dieterich, W. Gebhardt, and M. Cardona, High pressure x-ray investigations of phase transitions in $\text{Cd}_{1-x}\text{Mn}_x\text{Te}$, *Solid State Commun.* **56**, 563 (1985).
- [58] S. Hull and D. A. Keen, High-pressure polymorphism of the copper(I) halides: A neutron-diffraction study to ~ 10 GPa, *Phys. Rev. B* **50**, 5868 (1994).
- [59] Z. Vardeny and O. Brafman, Disorder-induced TA Raman lines in mixed Cu-halide crystals, *Phys. Rev. B* **19**, 3290 (1979); the data from this reference on $\text{CuCl}_x\text{Br}_{1-x}$ ($x = 0.95-0.04$) are used in the present study].
- [60] J. Serrano, M. Cardona, T. M. Ritter, B. A. Weinstein, A. Rubio, and C. T. Lin, Pressure and temperature dependence of the Raman phonons in isotopic γ -CuI, *Phys. Rev. B* **66**, 245202 (2002).
- [61] J. Gonzalez, B. J. Fernandez, J. M. Besson, M. Gauthier, and A. Polian, High-pressure behavior of Raman modes in CuGaS_2 , *Phys. Rev. B* **46**, 15092 (1992).
- [62] A. A. Correa, S. A. Bonev, and G. Galli, Carbon under extreme conditions: Phase boundaries and electronic properties from

- first-principles theory, *Proc. Natl. Acad. Sci. USA* **103**, 1204 (2006), and references therein.
- [63] J. Xie, S. P. Chen, J. S. Tse, S. de Gironcoli, and S. Baroni, High-pressure thermal expansion, bulk modulus, and phonon structure of diamond, *Phys. Rev. B* **60**, 9444 (1999).
- [64] M. T. Yin and M. L. Cohen, Will Diamond Transform under Megabar Pressures? *Phys. Rev. Lett.* **50**, 2006 (1983).
- [65] M. T. Yin, Si-III (BC-8) crystal phase of Si and C: Structural properties, phase stabilities, and phase transitions, *Phys. Rev. B* **30**, 1773 (1984).